Journal of Nuclear Materials 396 (2010) 181–188

Contents lists available at ScienceDirect

Journal of Nuclear Materials

journal homepage: www.elsevier.com/locate/jnucmat

Porosity effects on the neutron total cross section of graphite

Sergio Petriw, J. Dawidowski *, Javier Santisteban

Consejo Nacional de Investigaciones Científicas y Técnicas, Centro Atómico Bariloche and Instituto Balseiro, Comisión Nacional de Energía Atómica, Universidad Nacional de Cuyo, 8400 Bariloche, Argentina

ARTICLE INFO

Article history:
Received 23 September 2009
Accepted 2 November 2009

ABSTRACT

For subthermal neutron energies, polycrystalline graphite shows a larger total cross section than predicted by existing theoretical models. In order to investigate the origin of this discrepancy we measured the total cross section of graphite samples of three different origins, in the energy range from 0.001 to 10 eV. Different experimental arrangements and sample treatments were explored, to identify the effect of various experimental parameters on the total cross section measurement. The experiments showed that the increase in total cross section is due to neutrons scattered around the forward direction. We associate these small angle scattered neutrons (SANS) to the porous structure of graphite, and formulate a very simple model to compute its contribution to the total cross section of the material. This results in an analytic expression that explicitly depends on the density and mean size of the pores, which can be easily incorporated in nuclear library codes.

1. Introduction

Graphite has been used in nuclear reactors since the birth of the nuclear industry due to its good performance as a neutron moderator material. Graphite is still an option as moderator for generation IV reactors due to its good mechanical and thermal properties at high operation temperatures [1]. So, there has been renewed interest in a revision of the computer libraries used to describe the neutron cross section of graphite [2–5].

A typical feature in the measured total cross sections of polycrystalline graphite found in the literature are the discrepancies between experimental total cross section in the low-energy region and the theoretical calculations commonly employed, as shown in Fig. 1. Such differences have been reported on nuclear-grade graphites of different origins by several groups [6–8,5]. Whilst the difference between the first Bragg edge (at 0.0018 eV) and 0.03 eV can be ascribed to the crystallographic texture of the material, there is yet no satisfactory explanation for the cross section measured at energies below the first Bragg edge. So, whilst the combined effect of nuclear absorption, incoherent and inelastic scattering predicts a value of nearly 0.2 b, the experimental values are typically over 4 b. The only exception is highly oriented pyrolityc graphite, which is polycrystalline but possesses near theoretical density and degree of orientation close to a single crystal, which shows a total cross section similar to the theoretical value [8–10]. Six decades after the first reports, there is still some controversy about the origin of the measured total cross section of graphite for low-energy neutrons.

In an early paper, Egelstaff [7] ascribed the origin of such an increase in the total cross section to small angle scattering of the neutrons due to refraction of the neutron beam as it passes through the many air/solid interfaces in the porous graphite. This explanation agreed with the experimental observation that an initially collimated neutron beam increases its divergence after passing through a graphite block [11]. In that work, Egelstaff briefly described two experimental arrangements aimed to subtract this small angle contribution, as he was mainly interested in the inelastic cross section and in the elastic cross section due to reflection on the crystallographic planes. By the same time, Antal et al. also recognized this 'porosity' scattering and performed similar corrective tests on experiments dedicated to study lattice defects in graphite, which also manifest as an increase in the total cross section for low-energy neutrons [12]. In a recent work, Bowman et al. [5] discarded the 'small angle' explanation and strongly criticized Egelstaff's experiments, reinterpreting Egelstaff account of the results, but without repeating the actual experiments.

In this work we study the origin of this discrepancy, by measuring the total cross section of room temperature graphite in the energy range from 0.001 to 10 eV, and compare it with standard calculation tools. To do so, we performed experiments on graphite samples from three different origins, studying the dependence of the total cross section with the geometry, orientation and dimensions of the actual sample. Besides this, we measured the total cross section of samples 'as received' and after an annealing treatment, to assess possible contributions due to scattering in lattice defects as discussed by Antal et al. [12]. Finally, in order to identify

* Corresponding author. Tel.: +54 2944 445165; fax: +54 2944 445299.
E-mail address: javier@cab.cnea.gov.ar (J. Dawidowski).

0022-3115/$ - see front matter © 2009 Elsevier B.V. All rights reserved.
doi:10.1016/j.jnucmat.2009.11.003

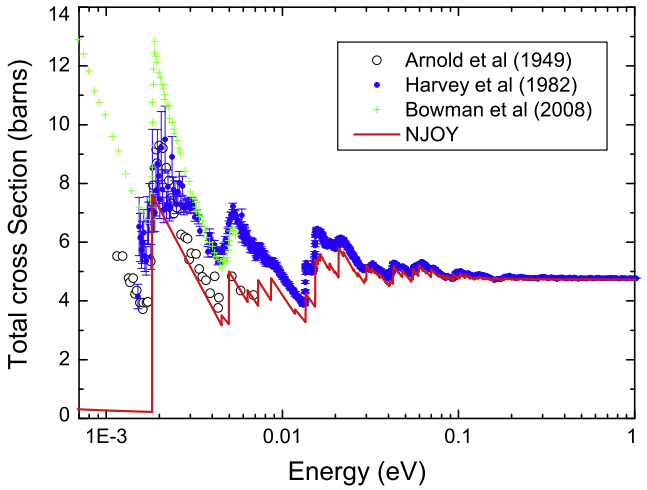

Fig. 1. Comparison of measured graphite total cross sections of different authors (cited in text [6,8,5]) with calculation performed with the NJOY code.

the contribution from small angle neutron scattering (SANS) we repeated Egelstaff work, by performing transmission experiments using two geometric configurations. The outcome of the experiments convinced us that the increase in the total cross section at subthermal neutron energies results indeed from small angle scattering in the porous graphite.

As mentioned, existing computer libraries of nuclear data provide evaluated values which differ from the actual measurements for polycrystalline graphite in the subthermal range. In particular, the very popular NJOY calculation code [13] includes a model for graphite with a detail of its crystal structure (elastic coherent term) as well as the vibrational modes of the lattice (inelastic term) [14]. However the code does not include any description of the 'mesoscopic' structure of the material such as porosity or voids, mainly because no theoretical model for the SANS total cross section has been developed so far. So, in the last section of this work we provide such a model of the total cross section, by assuming a very simple description about the distribution of the pores. We consider spherical air pores uniformly distributed in graphite, which results in an analytic expression for the total cross section that explicitly depends on the density and mean size of the pores. Finally, we show that the experimental total cross section of polycrystalline graphite can be effectively described by simply adding an analytic SANS component to the usual theoretical approach implemented in NJOY.

2. Experimental

2.1. Samples

Virtually all nuclear graphites are manufactured from petroleum or pitch cokes, binded and impregnated with different materials. By variation of these ingredients and the forming and final heat treatment, it is possible to produce a wide range of physical properties and behaviors under irradiation. In this work, samples of various geometries and sizes were produced from nuclear-grade graphites of three different types, namely 'needle-coke graphite', 'pitch coke graphite' and 'isostatically pressed graphite'.

2.1.1. Needle coke graphite

Needle coke graphite is widely used in the manufacture of electrodes in the metallurgical industry and corresponds to the most porous material. Because of its availability and purity it was used in the manufacture of the first moderator materials during the development of nuclear fission reactors [15]. This material has a large anisotropy, which caused some problems after long exposures to radiation. Samples were cut from a 24 cm cube provided by the RA-6 Nuclear Reactor, Centro Atómico Bariloche, Argentina. The density of the material we used is (1.681 ± 0.008) g/cm^3. An EXAFS analysis provided a composition (C 99.815%, S 0.102%, Ca 0.047%, Si 0.026%, Al 0.009% and K 0.001%). Pores of around 1 mm were visible to the naked eye. A micrograph of the surface of these materials is shown in Fig. 2.

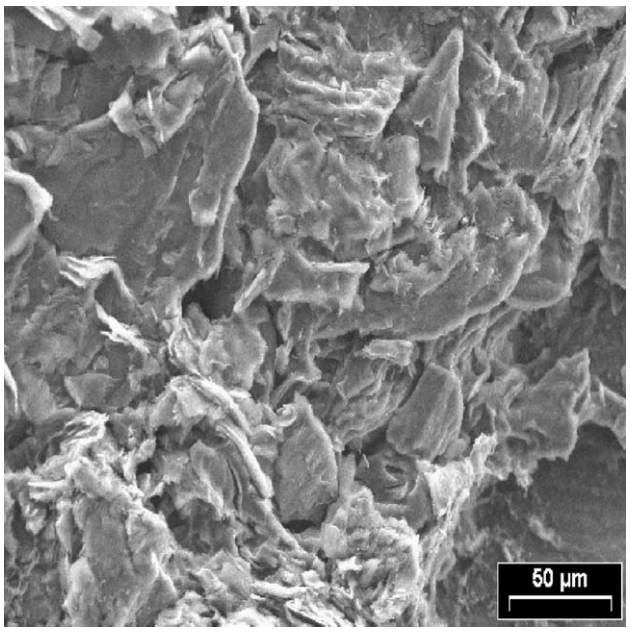

Fig. 2. Micrograph of the surface of the needle-coke nuclear-grade graphite cube studied in this work.

2.1.2. Pitch coke graphite

Pitch coke graphite is produced by heat treatment of the higher molecular weight products of pitch production, leading to more isometric particles than needle-coke graphite. The material used is more dense (1.725 ± 004) g/cm^3 than the needle-coke graphite. The sample presents a smoother surface than pitch coke graphite, but the pores are still visible to the naked eye. Spherical samples were machined out from a rod.

2.1.3. Isostatic-pressed graphite

Isostatic-pressed graphite uses finer coke particles and allows the manufacture of a wide range of isotropic graphites having very uniform and isotropic properties, which may be used as moderator materials. Spherical samples were moulded by isostatic pressing. These samples presented the largest density (1.740 ± 004) g/cm^3.

Table 1 describes the samples used on these experiments. The density of each sample was determined from its weight and volume. The porosity was calculated by comparison to the theoretical density for graphite $\rho_C = 2.266$ g/cm^3 and the measured densities ρ_a. The total volume of the pores is

$$V_P = M\left(\frac{1}{\rho_a} - \frac{1}{\rho_C}\right), \tag{1}$$

and the porosity

$$P = V_P/V_T, \tag{2}$$

where V_T is the total sample volume.

The values of the calculated porosities (shown in Table 1) are in the range of variation observed on graphites (between 7% and 30% [16]).

Table 1
Summary of the three types of samples studied in this work.

Sample	Dimensions (cm)			Mass (g)	Density (g/cm^3)	Porosity (%)
	Shape	Thickness	Diam./Width			
Pitch coke	Sphere	–	6.00	195.3	1.725 (4)	23.9
Isostatically pressed	Sphere	–	6.00	196.8	1.740 (4)	23.2
Needle coke	Cylinder	8.27	4.18	191.32	1.681 (8)	25.8

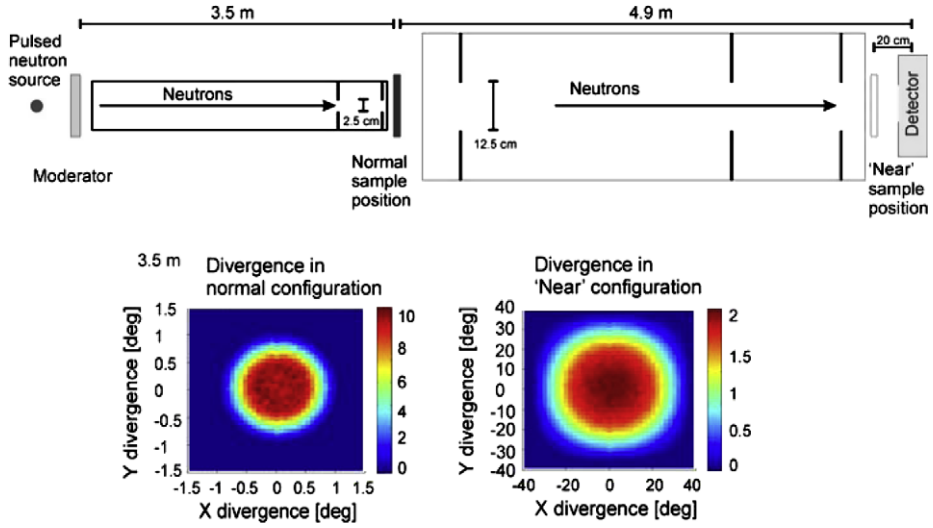

Fig. 3. General scheme for the transmission experiments. The "normal" and "near" sample positions are shown (see text for details). Distances are expressed in metres. (Bottom) The neutron beam divergence at the detector position for each experimental arrangement.

2.2. Neutron transmission

The total cross section of the samples was measured by transmission experiments performed at the Bariloche electron linear accelerator (LINAC) facility (Argentina). A general scheme of the transmission experimental setup is shown in Fig. 3. The accelerator operated at a frequency of 50 Hz, and a 25-μA mean electron current. Neutrons, produced by the interaction of the electrons accelerated by the LINAC on a lead target, were moderated in a 20 mm thick polyethylene slab. Measurements were carried out at room temperature, employing the "sample in-sample out" technique [17] every 10 min. The detector bank consisted of seven ^{3}He proportional counters (10 atm filling pressure, 6 in. active length, 1 in. diameter) placed on the incident beam path at 8.27 m from the neutron source. The sample was at a distance of 4.9 m from the detection bank. The beam was circular, with a diameter of 25 mm at a distance of 3.5 m from the moderator. The neutron beam was collimated, so its cross sectional diameter was 12.5 cm at the detection position. An independent detector placed near the neutron source was employed as a monitor, which served to normalize the spectra. The background contribution was determined with a polyethylene beam stop covered with cadmium at the sample position.

Fig. 4 shows typical spectra measured during the experiments, where the three energy regions of interest, i.e., the epithermal, thermal and subthermal ranges have been identified. The 'sample' spectrum in the figure corresponds to the needle-coke graphite, and clearly displays the characteristic Bragg edges in the subthermal range. We have adopted different energy resolutions for each energy range. For the thermal range, where the count rate is higher, we used $\Delta E/E = 0.01$ whilst we used $\Delta E/E = 0.03$ in the subthermal range and $\Delta E/E = 0.05$ in the epithermal range. The total cross section of the material is calculated from the transmission resulting from the spectra shown in the figure. If $\Phi(E)$ is the incident spectrum, $S(E)$ is the spectrum transmitted by the sample and $B(E)$ is the background, the transmission is determined from

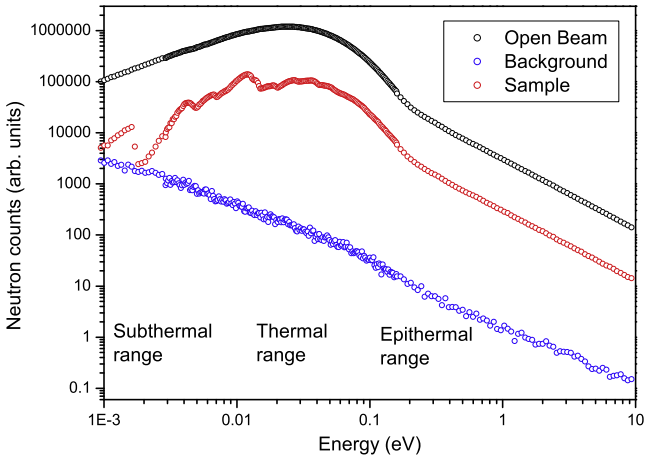

Fig. 4. Spectra of open beam, background and transmitted beam from the needle-coke graphite in the "normal" position as a function of the energy. The intensity is expressed in the rate of number of counts over monitor counts.

$$T(E) = \frac{S(E) - B(E)}{\Phi(E) - B(E)}, \tag{3}$$

and the total cross section $\sigma_{tot}(E)$ is

$$\sigma_{tot}(E) = -\frac{A}{\rho_a t N_A} \ln(T(E)), \quad (4)$$

where ρ_a is the sample density (employed in Eq. (1)), A is the atom mass, t the sample thickness and N_A Avogadro's number. For the spherical samples, the sample thickness varies across the neutron beam area, so the average thickness (5.71 cm) was adopted for the calculation of the total cross section from the measured transmission.

2.3. Measurements

In order to assess the effects of anisotropy on the total cross section of the different graphites we measured the transmission along three mutually perpendicular directions. For the needle-coke graphite we used a cubic sample of 5 cm side. Previous works showed that the transmission of thermal neutrons through anisotropic materials depends on the neutron energy and the orientation of the sample [6,7,18].

Antal et al. [12] reported large changes in the low-energy total cross section of graphite due to radiation damage, presumably as a result of the creation of vacancies in the crystal lattice. The effect is reversible, and the total cross section falls to normal values after an annealing treatment. In order to assess the effect of pre-existing vacancies on the total cross section, we measured the transmission of needle-coke samples in the 'as received' state, and after an annealing treatment at 900° in an argon atmosphere during 5 h. We performed measurements on two pairs of samples, cubic samples of 5 cm side, and cylindrical samples of 1 cm thickness and 4.2 cm diameter.

As discussed in the Introduction, several authors have pointed out to small angle scattering as the reason of the increase in the total cross section at low energies. In order to isolate the contribution of these small angle scattered neutrons to the total cross section we repeated the measurements on the needle-coke graphite, but using a slab sample of 2.57 cm thickness. We performed two measurements: a first measurement using the normal experimental arrangement described above; and a second measurement placing the slab just in front of the detector, as shown in Fig. 3. The main difference between the 'normal' configuration and this 'near' configuration resides in their acceptance to the neutrons that have suffered collisions within the sample. This difference can be effectively quantified in terms of an acceptance angle, which is described in the following section.

Finally, we also studied the dependence of the total cross section on the thickness of the actual sample. For this, we produced samples of the needle-coke graphite of five different thicknesses which are listed in Table 2.

2.4. Experimental results

Fig. 5 shows the result of the total cross section measured for the three different graphites referred in Section 2.1. On the epithermal range, all samples tend to a value σ_{epi} quite close to the free-atom cross section of graphite ($\sigma_{free} = 4.75$ b) (Table 3). All samples display the Bragg edges characteristic of polycrystalline material. The three curves start to separate from each other at 0.01 eV, and the difference between them seems to increase in inverse form to neutron energy.

The height of the first Bragg edge, i.e., the (0002) is proportional to the number of crystallites having their basal planes perpendicular to the neutron beam direction. The large error bars obtained for energies slightly larger than this Bragg edge are due to a very low sample transmission at such energies, resulting in a measured signal quite close to the background level (see Fig. 4). Table 3 lists the cross sections for energies just below the (0002) Bragg edge (σ_{sub}) and the height of this edge ($\Delta\sigma$ (0002)) for each sample. The value expected for a randomly oriented polycrystal is 7.4 b. The values measured for the present samples differ from this

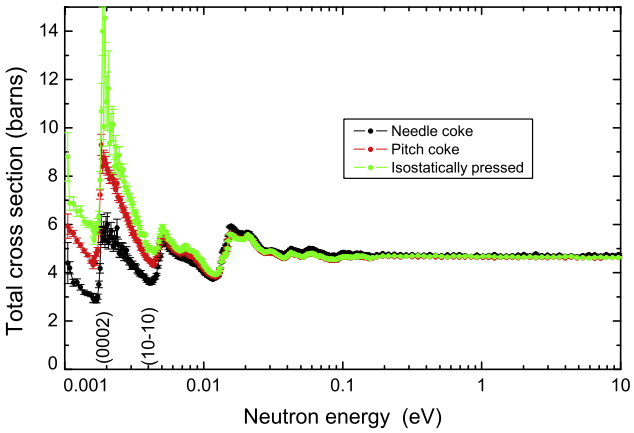

Fig. 5. Total cross section of three different nuclear-grade graphites.

Table 2
Characteristics of the needle-coke graphite samples studied in this work.

Sample	Dimensions (cm)			Mass (g)
	Shape	Thickness	Diam./Width	
Needle coke 1	Cylinder	8.27	4.18	191.32
Needle coke 2	Cylinder	1.34	4.15	30.76
Needle coke 3	Cylinder	1.4	4.18	32.1
Needle coke 4	Cylinder	1.08	4.17	24.7
Needle coke 5	Slab	2.57	18.00	1150
Needle coke 6	Cube	5	5.00	210

Table 3
Details about the cross sections measured on the different graphite samples. σ_{epi}: cross sections for epithermal energies; σ_{sub}: cross sections for energies just below the (0002) Bragg edge; $\Delta\sigma$ (0002): Height of the (0002) Bragg edge.

Sample	Cross sections (barns)			
	σ_{epi}	σ_{sub}	$\Delta\sigma$ (0002)	$\Delta\sigma_{aniso}$
Isostatically pressed	4.7 (1)	5.7 (1)	6.3 (9)	0.7
Pitch coke	4.6 (1)	4.4 (1)	5.2 (5)	2.9
Needle coke	4.70 (5)	2.95 (7)	3.4 (3)	1.5

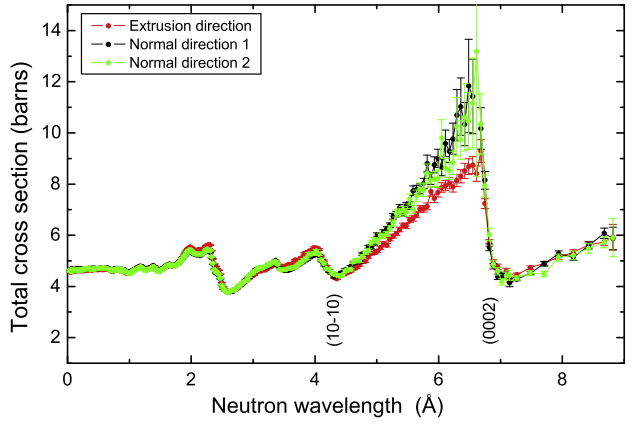

Fig. 6. Total cross section of the pitch coke graphite sphere, determined for three mutually perpendicular neutron incidence directions.

theoretical value and between each other. This is due to the anisotropy, or crystallographic texture, resulting from the different manufacturing processes.

The anisotropy of the samples also manifests as change in the total cross section measured along different directions of the specimen. Fig. 6 shows the total cross section of the pitch coke graphite along three mutually perpendicular directions, one of them corresponding to the extrusion direction of the block. The curves are presented in terms of neutron wavelength rather than neutron energy, because the differences manifest more clearly using this scale. Neutron wavelength is also a more natural scale, as the Bragg edges occur due to neutrons elastically reflected on the crystallographic planes of the sample. In the figure, the extrusion direction starts separating from the other curves near the (10–10) Bragg edge; but perfectly agrees with them for wavelengths longer than 6.72 Å, after the (0002) Bragg edge. The total cross section between 4.24 Å and 6.72 Å directly depends on the orientation distribution of basal planes. This effect has been studied in the early works of Refs. [6,7]. The present results show a smaller total cross section along the extrusion direction, in accordance with Ref. [7]. The maximum difference observed between the height of the (0002) Bragg edges measured along different directions for each sample ($\Delta\sigma_{aniso}$) is reported in Table 3, as a rough indicator of the anisotropy of the sample. The fact that the three directions perfectly agree beyond the (0002) Bragg edge indicates that the physical process responsible for the increase in total cross section at subthermal energies is of isotropic nature.

Similar results were observed for the needle-coke graphite, but the differences between directions were slightly smaller in this case. On the other hand, the isostatically pressed graphite presented virtually the same total cross section for all three directions, within the uncertainty of the measurement. This reflects the more isotropic material obtained from this manufacturing process. The difference $\Delta\sigma_{aniso}$ between directions reported in the table falls within the uncertainty of the measurement.

The total cross section of the needle-coke graphite was essentially the same for the 'as-received' and after an annealing treatment. This discarded scattering in lattice vacancies as a possible explanation for the discrepancy in total cross section we are interested in.

Fig. 7a shows the transmission of the slab sample of needle-coke graphite measured in the normal configuration (solid symbols), and in the 'near' configuration, i.e., with the slab placed just in front of the detector bank (open symbols). The main difference between these measurements resides in their acceptance angle to the neutrons that have undergone collisions within the sample. In the near configuration, neutrons scattered at low-angles are counted by the detector and manifest as an apparent increase in the transmission of the sample.

In order to define an acceptance angle characteristic of each configuration, we performed Monte Carlo simulations of the experimental arrangements using the computer code MCSTAS [19,20]. In both cases we considered an isotropic scatterer, and a detector having a diameter of 12.5 cm. The effective diameter of the sample was determined by the size of the neutron beam at the sample position, which increases with the distance from the moderator as a result of the neutron beam divergence.

In the 'normal' configuration, the sample diameter is 2.5 cm at 490 cm from the detector, whilst in the 'near' configuration the sample diameter is 12 cm at 20 cm from the detector. The insets in Fig. 3 show the distribution of angular divergence of the neutrons arriving at the detector for the two configurations. As expected, both distributions are centrosymmetric and centred at the origin. We have defined the acceptance angle α as the half-width at half-maximum of the angular divergence distribution. For the 'normal' case we obtain an acceptance angle of just 0.7°, whilst for the 'near' case α reaches a value of 25°.

A 'pseudo' total cross section (σ_{pseudo}) can be evaluated via Eq. (4) from the transmission measured in the 'near' configuration, as shown by the solid symbols in Fig. 7b. This is a 'pseudo' total cross section in the sense that this total cross section does not include any scattering processes deflecting neutrons within a 25° cone around the incident neutron beam. As expected, it can be appreciated that the curve of σ_{pseudo} is always below the total cross section for the needle-coke graphite presented in Fig. 5. We can also appreciate that the value of σ_{pseudo} falls to almost zero for wavelengths longer than the (0002) Bragg edge. This means that if a neutron of this wavelength were to be scattered by the sample, it would be deflected by an angle smaller than 25°.

On the other hand, we can experimentally define the total cross section σ_{SANS} associated with the neutrons scattered by needle-coke graphite between 0.7° and 25° by comparing the transmission T_{near} measured on the 'near' configuration with the value T_{normal} measured with the normal configuration,

$$\sigma_{SANS}(E) = -\frac{A}{\rho t N_A}\{ln(T_{normal}(E) - ln(T_{near}(E))\}, \quad (5)$$

The curve of σ_{SANS} is given by the open symbols in Fig. 7b. This contribution to the total cross section remains nearly constant at a value of 1 b between 1 Å and 4 Å, where it starts increasing with neutron wavelength. This means that as the neutron wavelength increases the scattering becomes more anisotropic, in the sense that a larger fraction of neutrons are scattered towards the forward direction. For wavelengths longer than the (0002) Bragg edge, this

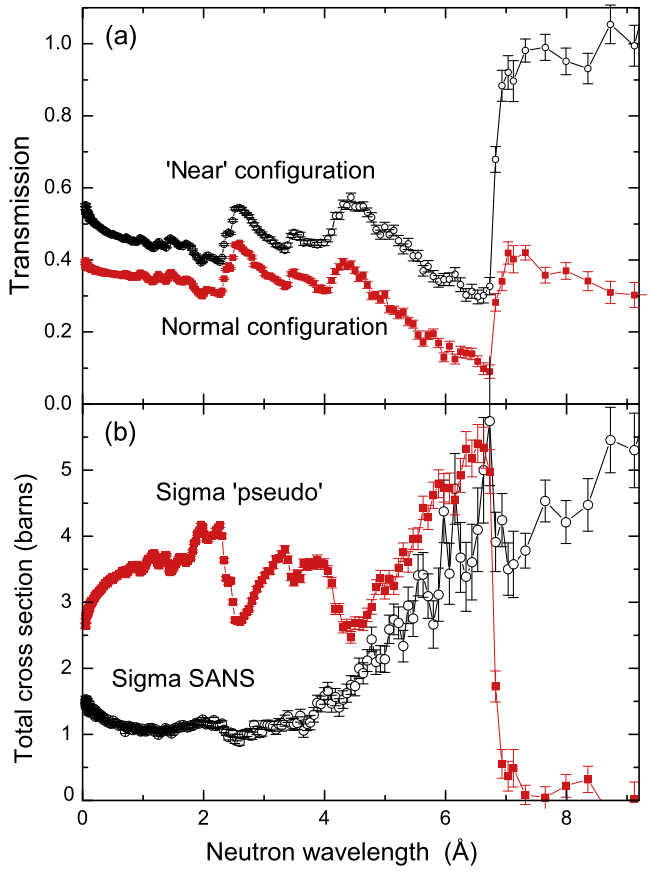

Fig. 7. Transmission of the slab sample of needle-coke graphite measured in the normal configuration (solid symbols), and in the 'near' configuration. (b) σ_{pseudo} (filled symbols) and σ_{SANS} (open symbols) calculated from Eq. (5).

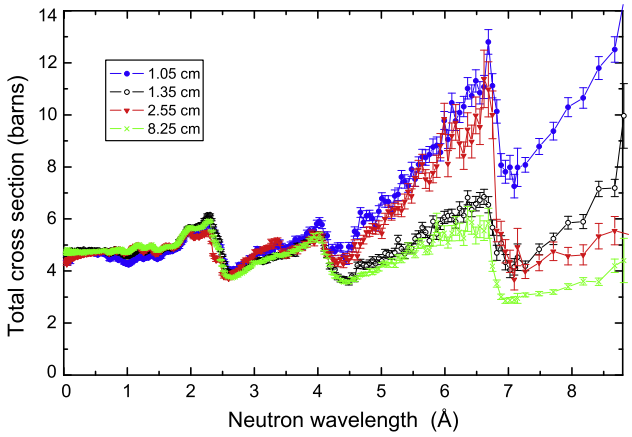

Fig. 8. Total cross section of needle-coke graphite of different thicknesses.

seems to be the only scattering process still active in the present sample. As expected, the forward contribution to the scattering also increases for wavelengths shorter than 1 A, which is mirrored by a decrease in σ_{pseudo}. This is because, as the energy of the neutron increases the free atom cross section becomes more anisotropic.

Fig. 8 shows the results of the total cross section for a series of needle-coke graphite samples of different thicknesses. Quite surprisingly, the curves present large differences for wavelengths longer than the (10–10) Bragg edge. The differences observed for wavelengths between this edge and the (0002) edge can be partially ascribed to crystallographic texture, as the samples were cut along different directions of the original block. For wavelengths longer than the (0002) edge, the total cross section increases with the decrease in sample thickness. Measurement were performed for pairs of nearly identical samples of 8.25 cm and and 1 cm. The thicker samples showed essentially the same total cross section, whilst the thin samples showed differences as large as 3 b in the long wavelength range. This indicates that the total cross section measured for relatively thin samples is quite dependent on sample features which are yet to be investigated.

2.5. Discussion

The present experiments have corroborated that the total cross section of polycrystalline graphite samples includes a low-energy contribution which is presently not considered in standard nuclear libraries.

This contribution to the total cross section is due to scattering occurring mainly in the forward direction, and it is dependent on the specific type of graphite. The experimental information is poorly defined for relatively thin samples.

There are three main candidates to explain an increase of total cross section at low neutron energies.

The presence of impurities with a very high absorption cross section can be discarded, because this unknown contribution disappeared when the slab was placed near the detector. An increased absorption is also very unlikely from a practical point of view, as the present graphites were intended to be used in nuclear applications.

The presence of impurities in the form of hydrogenous substances is a real possibility, as humidity from the air and residues from the binder used in the manufacturing of graphite are almost certainly present in all samples. Hydrogen displays anisotropic scattering towards the forward direction at high energies, but the scattering at low energies is expected to be quite isotropic.

We estimated the humidity absorbed from the air by drying a needle-coke sample at 200 C during 7 h, and monitoring the weight increase when exposed to air at room temperature. After 150 min the weight increase stabilized on a value of 0.024%. Taking σ_{water} around 200 b as the low-energy cross section of water, we obtain a rough contribution of 0.05 b, which is clearly too low to explain the observed effect.

Regarding the remains of the manufacturing process, we can estimate the concentration of binder remains x_i compatible with the observed increase in total cross section. We consider that the total cross section of the binder is essentially given by the average number of protons N_H in the binder molecular unit, times the bound-atom cross section of hydrogen, $\sigma_H = 82$ b. On doing this we are simplifying the effect of chemical binding on the total cross section of the proton. Assuming a similar density for the binder and the graphite, we obtain the concentration of binder as

$$x_i = \frac{\Delta\sigma_{exp}}{N_H \sigma_H}, \tag{6}$$

where $\Delta\sigma_{exp} = 5.5$ b is the difference between the experimental and theoretical values. For an average of five protons per binder molecule, we conservatively estimate that a 1% in weight in hydrogenous impurities could explain the observed difference However, such concentration seems unfeasible, as typical nuclear graphites have 99.9% purity, and only half of the impurities may be hydrogenous in nature.

The third possibility is the scattering in the large number of pores typically present in graphite, which is discussed in detail in the next section.

3. Porosity small angle scattering

The experimental results presented showed that small angle scattering effects are responsible for the discrepancies observed between experimental and theoretical calculations in the total cross section of graphite. In this section we will formulate a simple small angle scattering model to relate the small angle effects observed and the porosity of the sample.

The models of small angle neutron scattering are formulated over $I(q)$ (the scattered neutron intensity sample as a function of q) where as usual $\mathbf{q} = \mathbf{k}_0 - \mathbf{k}$, and $\mathbf{k}_0$ and $\mathbf{k}$ are the incident and emergent neutron wave vectors, respectively. The intensity will depend only on the modulus of $\mathbf{q}$ in the case of isotropic sample. Since the measured magnitude is the total cross section we will firstly show its relationship with $I(q)$. Based on Ref. [21] we write the microscopic total cross section as

$$\sigma(k_0) = \frac{\sigma_b}{2k_0^2} \int_0^\infty q\, dq \int_{\varepsilon_{min}}^{\varepsilon_{max}} S(q,\varepsilon) d\varepsilon, \tag{7}$$

where σ_b is the bound-atom cross section, $\varepsilon = E_0 - E$ the difference between the incident and the emergent neutron energy. In Eq. (7) ε_{min} and ε_{max} are the limits of the kinematic range [21] accessible for a given q. In a solid the scattering is mainly elastic, so the integrand in energies (ε) is significant only around $\varepsilon = 0$, and the result of the integral is $I(q)$ (identified with $\sigma_b S(q)$). The q-range of integration in the elastic regime extends from 0 to $2k_0$, resulting

$$\sigma(k_0) = \frac{1}{2k_0^2} \int_0^{2k_0} q\, I(q)\, dq, \tag{8}$$

that is the sought relationship.

In the literature (e.g. Ref. [22]) different models are formulated for the small angle intensity $I(q)$ of two-phase systems. We are interested in a dilute particulate system consisting in spherical air pores uniformly distributed in the graphite. The pore sizes can have a great variation according to the thermal treatment. In the literature we find a variation ranging roughly between 10

and 300 Å [16]. The energies where SANS is manifested that we are going to explore ranges between 1 and 5 meV, what means a wave-vector range from 0.7 to 1.6 Å^{-1}. If r_P is the mean pore size, we will explore an energy range where the product qr_P will be roughly greater than 2, up to several hundreds. In this limit it is valid to apply the Porod law

$$I(q) = \frac{2\pi(\Delta\rho)^2 s_P}{n q^4}. \tag{9}$$

Written in this form it will allow us to calculate the total cross section in barns, as we will show below. In Eq. (9) s_P is the total area of the boundaries between the two phases in the sample per unit volume, n the number density of atoms in the sample (that in this case is $n = n_C(1-P)$, where n_C is the theoretical graphite number density and P is defined in Eq. (2)), and $\Delta\rho$ (commonly called *contrast*), is the difference between scattering length densities of the two phases. In this case we will consider the interphase graphite–air. Neglecting the contribution of the air its value is

$$\Delta\rho = b_c \frac{\rho_C N_A}{M_C}, \tag{10}$$

where b_c is the carbon bound scattering length, N_A the Avogadro number, ρ_C the graphite theoretical density, and M_C the carbon atomic mass. Calculating this value with $b_c = 6.6484$ fm and the graphite theoretical density mentioned in Section 2.1.3 we obtain

$$\Delta\rho = 7.497 \times 10^{-6}\ \text{Å}^{-2}, \tag{11}$$

To formulate an elementary description of the pore structure, we will assume spherical pores of radius r_P, so the volume of a pore is $v_P = 4/3\pi r_P^3$, the number of pores is $N_P = V_P/v_P$, and the total surface is $S_P = N_P 4\pi r_P^2$, so the specific surface appearing in Eq. (9) results

$$s_P = \frac{3P}{r_P}. \tag{12}$$

We will now calculate the total cross section due to the small angle scattering produced by the pores starting from Eq. (8). As stated above, we will employ a Porod model in the high q region, however, since our integral includes also low q values where the Porod law cannot be applied, we will adopt a behavior according to the Guinier law in that region and both laws will be forced to match at $q = R_g^{-1}$ [22], where R_g is the *radius of gyration*, that for a sphere of radius r_P (the radius of the pores) is

$$R_g = \sqrt{\frac{3}{5}} r_P. \tag{13}$$

So the adopted $I(q)$ is

$$I(q) = \begin{cases} \dfrac{P}{1-P}\dfrac{A}{R_g q^4} & \text{if } q \geqslant R_g^{-1}, \\ \dfrac{P}{1-P} B \exp\left(-\dfrac{1}{3}q^2 R_g^2\right) & \text{if } q < R_g^{-1}, \end{cases} \tag{14}$$

where $A = 0.727531$ b Å^{-3} (calculated from Eqs. (9), (10), (12) and (13)) and $B = Ae^{1/3}R_g^3$ (calculated from the matching condition at $q = R_g^{-1}$). Employing this expression in Eq. (8)

$$\sigma(k_0) = \frac{P}{1-P} \times \frac{1}{2k_0^2}\left[\int_0^{R_g^{-1}} B\exp\left(-\frac{1}{3}q^2R_g^2\right) q\,dq + \int_{R_g^{-1}}^{2k_0} \frac{A}{R_g q^4} q\,dq\right]. \tag{15}$$

After solving the integrals and expressing as a function of the wavelength $\lambda_0 = 2\pi/k_0$ the result is

$$\sigma(\lambda_0) = \frac{P}{1-P}\frac{A}{8\pi^2}\lambda_0^2 R_g\left(\left(\frac{3}{2}e^{\frac{1}{3}} - 1\right) - \frac{\lambda_0^2}{32\pi^2 R_g^2}\right). \tag{16}$$

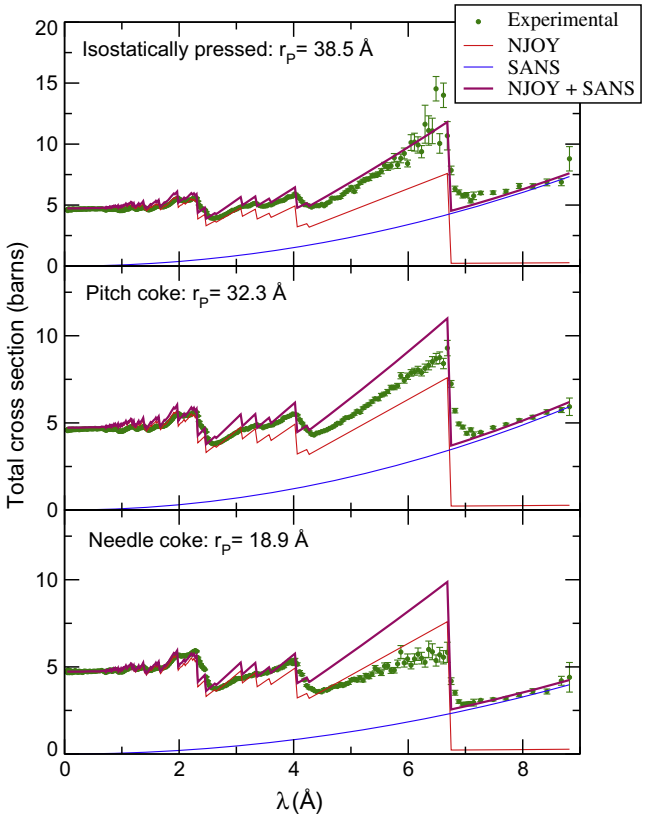

Fig. 9. Experimental total cross sections for isostatically pressed, pitch coke and needle-coke graphite compared with the SANS model plus the NJOY calculations whose contributions are also separately shown. The fitted pore radii are indicated.

Making explicit the numeric constants and the pore radius r_P (13), the expression is

$$\sigma(\lambda_0) = \left(7.13736 \times 10^{-3}\ \text{b Å}^{-3}\right)\frac{P}{1-P}\lambda_0^2 r_P\left(1.09341 - \frac{0.005277\lambda_0^2}{r_P^2}\right). \tag{17}$$

Eq. (17) has the pore radius as its single parameter, that can be fitted from the experimental data. In Fig. 9 we show the results after fitting Eq. (17) plus the NJOY calculations on the experimental data of isostatically pressed, pitch coke and needle-coke graphite. The fitted values are 38.5 ± 0.9 Å for isostatically pressed graphite, 32.3 ± 0.8 Å for pitch coke graphite and 18.8 ± 0.5 Å for needle-coke graphite. The lack of agreement between the calculations and the experimental data between the (10–10) and the (0002) Bragg edges for the last two systems is due to the texture effects above mentioned, that are not present for long wavelengths above the first Bragg edge. For this reason the data were fitted only in that range for pitch coke and needle-coke graphite, whereas the full wavelength range was employed for the isostatically pressed graphite.

4. Conclusions

The total cross section of a series of polycrystalline graphite samples was studied by transmission experiments. On the thermal range the total cross section is dominated by the contribution of the Bragg edges. For needle-coke and pitch coke graphites the cross section depended on the sample orientation, in agreement with previous works. On the other hand, the experimental cross section of isostatically pressed graphite was isotropic, indicating negligible crystallographic texture within the samples.

The experiments showed that the total cross section for sub-thermal neutron energies is mainly due to small angle scattering processes. The magnitude of this scattering depends on the type of graphite, but is independent of the sample orientation, at least for the three graphite types studied in this work.

We proposed a simple theoretical model that explains this small angle scattering in terms of scattering due to small angle scattering resulting from the graphite porosity. The model is based on a combination of the Porod and Guinier regimes to represent a set of spherical pores where the radius was a free parameter, that was fitted on the experimental data. The resulting values of the average pore sizes are within the pores sizes reported in the literature [16,23].

References

[1] A Technology Roadmap for Generation IV Nuclear Energy Systems, Tech. Rep. GIF-002-00, US DOE, December 2002. <http://www.gif.inel.gov/roadmap/>.
[2] I.I. Al-Qasir, A.I. Hawari, Transactions of the American Nuclear Society 96 (2007) 660–661.
[3] M. Adib, N. Habib, M. Fathaalla, Annals of Nuclear Energy 33 (2006) 627–632.
[4] T. Zhou, Benchmarking thermal neutron scattering on graphite, Ph.D. Thesis, North Caroline State University, 2006.
[5] C.D. Bowman, D.C. Bowman, T. Hill, J. Long, A.P. Tonchev, W. Tornow, F. Trouw, S. Vogel, R.L. Walter, S. Wender, V. Yuan, Nuclear Science and Engineering 159 (2) (2008) 182–198.
[6] G.P. Arnold, V.W. Myers, A.H. Weber, Physical Review 75 (2) (1949) 217–220, doi:10.1103/PhysRev.75.217.
[7] P. Egelstaff, Journal of Nuclear Energy 5 (1957) 203.
[8] J. Harvey, H. Mook, N. Hill, O. Shahal, Solid state effects on thermal cross-sections and on low energy resonances, in: K. Böckhoff (Ed.), International Conference on Nuclear Data for Science and Technology. Nuclear Data for Science and Technology, 1983 ECSC, EEC, EAEC, Brussels and Luxembourg, Nuclear Data for Science and Technology, 1982, pp. 961–964.
[9] B.O. Loopstra, Nuclear Instruments and Methods 44 (2) (1966) 181–187, doi:10.1016/0029-554(66)90149-2.
[10] K. Naguib, M. Adib, Annals of Nuclear Energy 25 (18) (1998) 1553–1563, doi:10.1016/S0306-4549(98)00052-8.
[11] D.J. Hughes, Neutron Optics, Interscience Publishers, Inc., 1954.
[12] J.J. Antal, R.J. Weiss, G.J. Dienes, Physical Review 99 (4) (1955) 1081–1085, doi:10.1103/PhysRev.99.1081.
[13] R.E. MacFarlane, D.W. Muir, The NJOY nuclear data processing system, Version 91, Los Alamos National Laboratory, October 1994.
[14] J.A. Young, J.U. Koppel, Physical Review 134 (6A) (1964) A1476–A1479, doi:10.1103/PhysRev.134.A1476.
[15] B.T. Kelly, B.J. Marsden, K. Hall, Irradiation damage in graphite due to fast neutrons in fission and fusion systems, Tech. Rep., International Atomic Energy Agency, Vienna, Austria, 2000.
[16] M. Bastick, P. Chiche, J. Rappeneau, X. Duval, Les Carbones par le Groupe Français détude des carbones, Masson et cie., in: A. Pacault (Ed.), Collection de chimie physique, 1965.
[17] F. Kropff, J.R. Granada, L.A. Remez, A. Vasile, Annals of Nuclear Energy 3 (1) (1976) 55–59.
[18] J.R. Santisteban, L. Edwards, V. Stelmukh, Characterization of textured materials by tof transmission, Physica B: Condensed Matter 385–386 (Part 1) (2006) 636–638, Proceedings of the Eighth International Conference on Neutron Scattering. doi:10.1016/j.physb.2006.06.090.
[19] P.O. Åstrand, K. Lefmann, E. Farhi, K. Nielsen, P. Skårup, New features in McStas, version 1.5, Applied Physics A 74(Suppl.) (2002) S1511–S1513.
[20] P. Willendrup, E. Farhi, K. Lefmann, Physica B: Condensed Matter 350 (1–3, Supplement 1) (2004) E735–E737.
[21] J. Dawidowski, J.R. Santisteban, J.R. Granada, Physica B: Condensed Matter 271 (1–4) (1999) 212–222, doi:10.1016/S0921-452(99)00216-1.
[22] R.-J. Roe, Methods of X-ray and Neutron Scattering in Polymer Science, Oxford University Press, 2000.
[23] D.L. Valladares, F.R. Reinoso, G. Zgrablich, Carbon 36 (10) (1998) 1491–1499, doi:10.1016/S0008-622(98)00141-9.